Chemical Engineering Science 138 (2015) 128–139

Contents lists available at ScienceDirect

Chemical Engineering Science

journal homepage: www.elsevier.com/locate/ces

Prediction of sizes and frequencies of nanoliter-sized droplets in cylindrical T-junction microfluidics

Shuheng Zhang [a], Carine Guivier-Curien [b], Stéphane Veesler [a], Nadine Candoni [a,*]

[a] Aix Marseille Université, CNRS, CINaM UMR 7325, 13288 Marseille, France
[b] Aix Marseille Université, CNRS, ISM UMR 7287, 13288 Marseille, France

HIGHLIGHTS

- Hydrodynamic of nanodroplets in a microfluidic system using a T-junction.
- Comparison of 3D cylindrical channels with 2D simulations using average velocity.
- Relation between size and frequency of droplets and total velocity, velocity ratio and Ca.

GRAPHICAL ABSTRACT

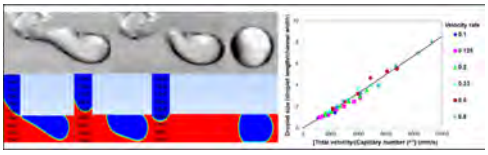

ARTICLE INFO

Article history:
Received 5 December 2014
Received in revised form
10 July 2015
Accepted 30 July 2015
Available online 10 August 2015

Keywords:
Microfluidic
Drop
Microreactor
Multiphase flow
Hydrodynamics
Fluid mechanics

ABSTRACT

We study the formation of nanoliter-sized droplets in a microfluidic system composed of a T-junction in PEEK and tubing in Teflon. This system, practical for a 'plug and play' set-up, is designed for droplet-based experiments of crystallization with a statistical approach. Hence the aim is to generate hundreds of droplets identical in size and composition and spatially homogeneous. Therefore, parameters of control are droplet size and frequency. However, the geometry of the T-junction is not perfect and, moreover, its channels are circular, as opposed to the planar geometries with rectangular cross-sections that are usually used. However, based on 3D experiments and 2D simulations, we observe the same regimes of droplet generation in circular channels as in planar geometries, and with the same stability. Therefore, we refer to velocities instead of flow rates to characterize the system. Then we define operating range in terms of droplet size and frequency through empirical relations using total velocity, velocity ratio and capillary number, to ensure homogeneous droplets in channels of 500 μm and 1 mm diameters.

1. Introduction

Nanoliter-sized droplets are increasingly used as nano-reactors in chemistry, for crystallization (Li et al., 2006; Selimovic et al., 2009), reaction (Li and Ismagilov, 2010) and analysis (Zare and Kim, 2010; Brouzes et al., 2009; Burns et al., 1998) studies. First, less material is consumed in nanoliter-sized droplets than in milliliter crystallizers. It is important to reduce material consumption when only small quantities of material are available, i.e. rare molecules such as pharmaceutical ingredients, purified proteins, or dangerous materials (energetic materials). Second, generating hundreds of nanoliter-sized droplets permits statistical analysis. Therefore microfluidic technologies are used with two-phase non-miscible flows, through flow-focusing (Gañán-Calvo and Gordillo, 2001; Anna et al., 2003), co-flowing (Umbanhowar et al., 1999; Garstecki et al., 2005) and cross-flowing (Thorsen et al., 2001; Garstecki et al., 2006). In our application, the microfluidic system is dedicated to droplet-based crystallization experiments. Nanoliter volumes makes it possible to nucleate a limited number of crystals that we can locate easily, and the generation of hundreds of nanoliter-sized droplets allows stochasticity of nucleation to be addressed Candoni et al. (2012). Therefore, our purpose is to generate hundreds of droplets identical in size and composition. Moreover, as we mix different solutions before the generation of

* Corresponding author. Tel.: +33 617248087.
E-mail address: candoni@cinam.univ-mrs.fr (N. Candoni).

http://dx.doi.org/10.1016/j.ces.2015.07.046
0009-2509/

droplets, the droplets' spatial homogeneity is also a crucial consideration.

In this paper, we study a 'plug and play' microfluidic system composed of a T-junction in PEEK and tubing in Teflon. Droplets are generated by cross-flowing the crystallization solution and the non-miscible oil, which is the continuous phase. The advantage of both Teflon and PEEK polymers over PDMS, which is only compatible with water, is their compatibility with organic solvents such as ethanol, acetone or nitrobenzene (Ildefonso et al., 2012). We choose ethanol as crystallization medium in order to ensure maximum versatility; we use as continuous phase fluorinated oil FC-70 which has no or very low miscibility with solvents like ethanol and good wettability with Teflon. Hence the shear of the continuous phase, which is injected into the junction perpendicular to the dispersed phase, leads to the break-up of dispersed phase droplets. We use Nemesys pumps to inject the continuous and the dispersed phase with reproducible flow rates, allowing us to generate droplets of the dispersed phase identical in size and frequency. Mixing inside droplets after their break-up is accelerated by the flow of the continuous phase if droplets can twirl in the channel, and hence the droplets are spatially homogeneous. But this twirling requires spherical droplets, which means that droplet diameter must be smaller than or equal to the channel diameter. However, droplets smaller than channel diameter can move in the channel and coalesce, depending on the frequency at which they are generated. The minimum droplet size must therefore be of the order of channel diameter and the frequency must be low.

The literature contains many experimental studies and simulations investigating the size of droplets. To the best of our knowledge, the studies presented in the literature use planar geometries with rectangular cross-section typically between 50 and 300 μm. They explore phase properties (viscosity (Garstecki et al., 2006; Xu et al., 2008; Christopher et al., 2008; Liu and Zhang, 2009; Gupta and Kumar, 2010; Glawdel et al., 2012a, 2012b; Chen et al., 2011; Wehking et al., 2013) and surface tension (Thorsen et al., 2001; Xu et al., 2008; Wehking et al., 2013), channel geometry (the height and the width of the channels (Garstecki et al., 2006; Glawdel et al., 2012a, 2012b; Wehking et al., 2013; Van Steijn et al., 2010)) and operating parameters (flow rate ratio (Garstecki et al., 2005, 2006; Xu et al., 2008; Christopher et al., 2008; Liu and Zhang, 2009; Gupta and Kumar, 2010; Glawdel et al., 2012a, 2012b; Chen et al., 2011; Van Steijn et al., 2010; Tice et al., 2003; Zhao and Middelberg, 2011)). Droplet size is shown to be influenced by flow rate ratio and capillary number (Garstecki et al., 2006; Xu et al., 2008; Christopher et al., 2008; Liu and Zhang, 2009; Wehking et al., 2013; Van Steijn et al., 2010; Tice et al., 2003; Zhao and Middelberg, 2011) (Ca). Moreover flow velocities are generally used instead of flow rates to represent droplet parameters (Xu et al., 2008; Christopher et al., 2008; Glawdel et al., 2012a, 2012b; Chen et al., 2011; Tice et al., 2003; Nisisako et al., 2002). To date, four distinct regimes of droplet formation or break-up within the confined geometry of a microfluidic T-junction have been described in the literature: squeezing, transient, dripping and jetting (Thorsen et al., 2001; Garstecki et al., 2006; Xu et al., 2008; De Menech et al., 2008). At low Ca, squeezing operates as a rate-of-flow-controlled regime, break-up arising from the pressure drop across the emerging droplet in the channel (Garstecki et al., 2006). At $Ca > 0.01$, dripping operates, shear stress playing an important role in break-up (Thorsen et al., 2001). Jetting operates at very high flow rates and/or with low surface tension (De Menech et al., 2008). An intermediate regime between squeezing and dripping, named transient, is observed by Xu et al. (2008) for $0.002 < Ca < 0.01$, in which break-up is controlled by both pressure drop and shear stress. But most authors did not use a transient regime and worked with a critical Ca of ≈ 0.015 to define the transition between squeezing and dripping (De Menech et al., 2008). In contrast, few studies deal with droplet frequency (Christopher et al., 2008; Gupta and Kumar, 2010; Wehking et al., 2013) even though it is easy to calculate using experimental results from the literature.

Our microfluidic configuration is easy to build and to use (Candoni et al., 2012; Ildefonso et al., 2012); it has circular channels, and the T-junction is not intended to be used for microfluidic experiments because its geometry is not perfect. Thus in this paper, we compare our non-perfect T-junction with circular channels to purpose-designed planar geometries with rectangular cross-sections molded in PDMS. We investigate the effect of total flow rate, flow rate ratios and capillary numbers on both droplet size and frequency. The aim is to define the operating range through empirical relations to ensure homogeneous droplets in channels of 500 μm and 1 mm diameters.

2. Material and methods

2.1. Experimental set-up

The microfluidic system (Fig. 1a) is composed of two tubings of identical internal diameter W (W is either 500 μm or 1 mm) made of Teflon. They are connected in a T-junction from IDEX in PEEK (polyether ether ketone) at right angles. The main channel contains the continuous phase (oil) whereas the orthogonal channel contains the dispersed phase (ethanol). The inner diameter of the T-junction is identical to that of the tubings, i.e. 500 μm or 1 mm (Fig. 1b).

The continuous phase and the dispersed phase are separately loaded using separate syringes placed in a syringe pump (neMESYS), which generates extremely smooth and pulsation-free fluid streams from 0.01 μL/s. The two phases are injected with given flow rates as follows: 0.15–12.3 μL/s for the continuous phase (Q_C) and 0.03–6.2 μL/s for the dispersed phase (Q_D). The ratio between the dispersed and the continuous flow rates (Q_D/Q_C) is varied from 0.1 to 0.8 and the total flow rate Q_{TOT} ($=Q_D+Q_C$) is varied from 0.28–14 μL/s. Variation in droplet size is 5% of the mean diameter, corresponding to 15% in terms of volume. However this variability is

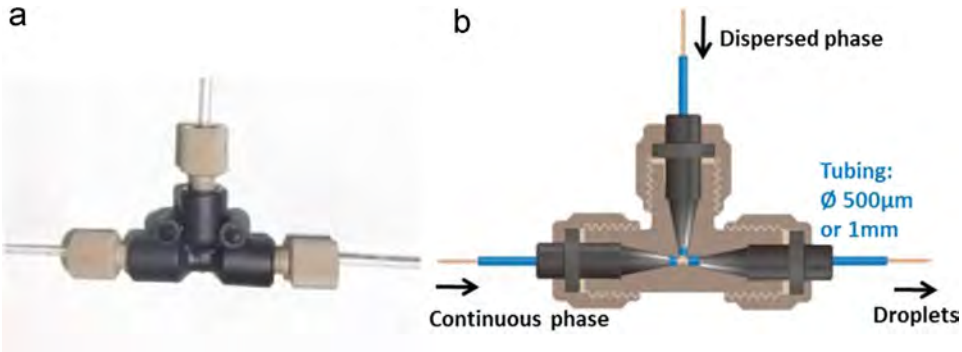

Fig. 1. (a) Photo and (b) scheme of PEEK T- junction from IDEX Health and Science catalog.

Table 1
Physico-chemical phase properties: density and dynamic viscosity are from the manufacturer's data sheet; surface tension is measured by the pendant drop method at 23 °C; contact angle is measured by the sessile drop method at 23 °C.

Phases	Density (kg/m^3)	Dynamic viscosity (Pa s)	Surface tension (mN/m)	Contact angle (°)
Continuous phase: fluorinated oil FC70 Dispersed phase: ethanol	$\rho_C = 1940$ $\rho_D = 789$	$\mu_C = 0.023$ $\mu_D = 0.0012$	$\gamma_{CD} = 6.7$	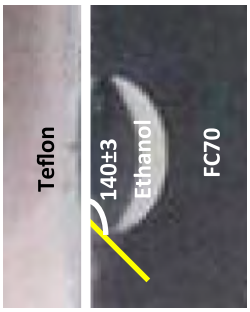

acceptable for chemical applications such as crystallization. Similarly, variability in droplet frequency is also acceptable because we are mainly interested in avoiding the coalescence of droplets.

2.2. Phase properties

The phases are fluorinated oil FC-70 for the continuous phase and ethanol for the dispersed phase. Fluorinated oil FC-70 (Hampton research) is chosen because it shows no or very low miscibility with ethanol and good wettability with the channel wall in Teflon, allowing droplets to be generated without addition of surfactants. Physico-chemical properties such as density, dynamic viscosity and surface tension are given in Table 1. The surface tension between the two phases is measured with the pendant drop method by forming droplets of ethanol in the oil at 23 °C, as previously described (Bukiet et al., 2012). Ethanol contact angle at FC-70/Teflon interface is measured at 23 °C.

2.3. Flow properties

The two phases are Newtonian. For a given T-junction geometry, the physico-chemical properties influencing droplet formation are density, dynamic viscosity, surface tension between the continuous and the dispersed phases, velocity of the flows and dimensions characteristic of the system, i.e. the radius of channels ($W/2$) (Zhao and Middelberg, 2011). We calculate the following parameters:

- The inertial forces and the viscous forces are compared through the Reynolds number, which is calculated using the continuous phase properties: its density ρ_C, viscosity μ_C and flow velocity v_C. It gives values of Re lower than 1, showing that the effect of inertia can be ignored:

$$\mathrm{Re} = \frac{\rho_C \times v_C \times (W/2)}{\mu_C} \tag{1}$$

  Thus the flow is laminar and their average velocity in our cylindrical microfluidic system is evaluated from the diameter W of channels and the flow rate Q as follows:

$$v = \frac{Q}{\pi (W/2)^2} \tag{2}$$

- The generation of droplets in a T-junction leads to the creation of a free interface between the two phases, characterized by the surface tension γ_{CD}. The corresponding capillary effects are in competition with gravity effects. The length above which gravity effects dominate capillary effects is the capillary length l_c:

$$l_c = \sqrt{\frac{\gamma_{CD}}{\Delta\rho \times g}} \tag{3}$$

  with g the gravity acceleration and $\Delta\rho$ the difference in density between the two phases. From the values of Table 1, $l_c = 2.4$ mm. Hence the gravity does not influence the deformation of the interfaces in millimetric or sub-millimetric channels.
- The *shear stress* and the surface tension are compared through the capillary number Ca. In the generation of droplets of a dispersed phase in a continuous phase, Ca is usually calculated using the average velocity v_C and viscosity μ_C of the continuous phase, and the surface tension γ_{CD}: (Thorsen et al., 2001; Garstecki et al., 2006; Xu et al., 2008; Christopher et al., 2008; Liu and Zhang, 2009; Gupta and Kumar, 2010; Wehking et al., 2013; Van Steijn et al., 2010; Tice et al., 2003; Zhao and

Middelberg, 2011).

$$\mathrm{Ca} = \frac{\mu_C \times v_C}{\gamma_{CD}} \quad (4)$$

Note that in this work μ_C and γ_{CD} are fixed. We have varied v_{TOT} $(=v_D+v_C)$ in a large range, i.e. more than one order of magnitude. And for a given v_{TOT}, we have varied the flow velocity ratio (v_D/v_C) from 0.1 to 0.8. Therefore, v_C is varied in almost two orders of magnitude.

2.4. 2D numerical simulations

2D numerical simulations are performed with software ANSYS and its computational phase dynamics package Fluent (version 12.1). The geometry is designed with DesignModeler, included in ANSYS software. The chosen geometry is a 2D T-junction similar to the experimental 3D geometry. The main channel is planar, with a width of 1 mm and a length of 20 mm. The secondary channel is similar, with the same width and 30 mm long. The entrance to the second channel is 30 mm away from the entrance to the main channel, assuming that the continuous phase is fully developed after 30 mm. Mesh is generated with meshing included in ANSYS software. A homogeneous structured mesh is used with 30 square cells per channel width.

Given that both phases are incompressible and immiscible, we choose the Volume of Fluid (VOF) model because it clearly describes the interface. Two-phase flows are fixed as laminar, unsteady and isothermal. The velocity and pressure fields are solved through the classical continuity equation and Navier–Stokes equation with the density ρ and the dynamic viscosity μ such that:

$$\rho = \phi_C\rho_C + \phi_D\rho_D \quad (5)$$

$$\mu = \phi_C\mu_C + \phi_D\mu_D \quad (6)$$

with ϕ_C and ϕ_D the volume fraction, ρ_C and ρ_D the density, and μ_C and μ_D the dynamic viscosity of continuous and dispersed phases respectively.

An additional source term F is added to the Navier–Stokes equation to take into account the interfacial tension through a continuum surface force model, with κ the interface curvature, $\vec{n}$ the interface outward normal vector and γ_{CD} the surface tension:

$$\vec{F} = 2\gamma_{CD} \times \frac{\rho\kappa\vec{n}}{(\rho_C+\rho_D)} \quad (7)$$

The governing equations are discretized to algebraic equations using a pressure based unsteady solver. The PRESTO! method is used for the pressure interpolation. The PISO algorithm and second-order upwind scheme is used for the pressure–velocity coupling and momentum equation respectively. A non-iterative time advancement (NITA) scheme is used in preference to a classical iterative time advancement scheme to speed up the simulation with equally accurate results. The time step is 10^{-4} s and the global courant number is kept under 2.

At the initial stage, the main channel is filled with the continuous phase and the secondary channel with the dispersed phase. The contact angle of droplets is set constant to 140° as ethanol contact angle at FC-70/Teflon interface is $140 \pm 3°$ (Table 1). Phase properties are the same as described in Section 2.2. The outflow condition for the outlet is chosen. At the inlet of each channel, a constant and flat velocity profile is imposed. This 2D numerical simulation is a preliminary feasibility test, which needs to be developed further. Additional numerical simulations will be realized, including 3D and complex geometries.

3. Results

Our aim is to define operating range in terms of droplet size and frequency to achieve homogeneous droplets in circular channels using our T-junction. We begin by comparing our circular 3D geometry to our 2D simulation. This 2D simulation yields the same results as the planar geometries generally used in the literature. Then we investigate the role of total flow rate, flow rate ratios and capillary numbers on both droplet size and frequency in order to establish empirical laws that will help in defining the operating range in channels of 500 μm and 1 mm diameters.

3.1. Relevance of velocities explored in 3D-experiments and in 2D-simulations

In this work, 2D simulations are carried out by controlling flow velocities as used in previous experimental studies to represent droplet parameters (Xu et al., 2008; Christopher et al., 2008; Glawdel et al., 2012a, 2012b; Chen et al., 2011; Tice et al., 2003; Nisisako et al., 2002). Here, the aim is to demonstrate that the displacement of phases in 3D cylindrical channels can be expressed by the average velocity instead of the flow rate, in a first approximation. In this way, experimental droplet generation in our cylindrical channels can be compared to the literature in which planar geometry with rectangular cross-section is used.

The experimental results are obtained by varying the flow rates of the continuous and the dispersed phases. In order to study the role of the total flow velocity v_{TOT} $(=v_D+v_C)$, the total flow rate Q_{TOT} $(=Q_D+Q_C)$ is varied in a large range, i.e. more than one order of

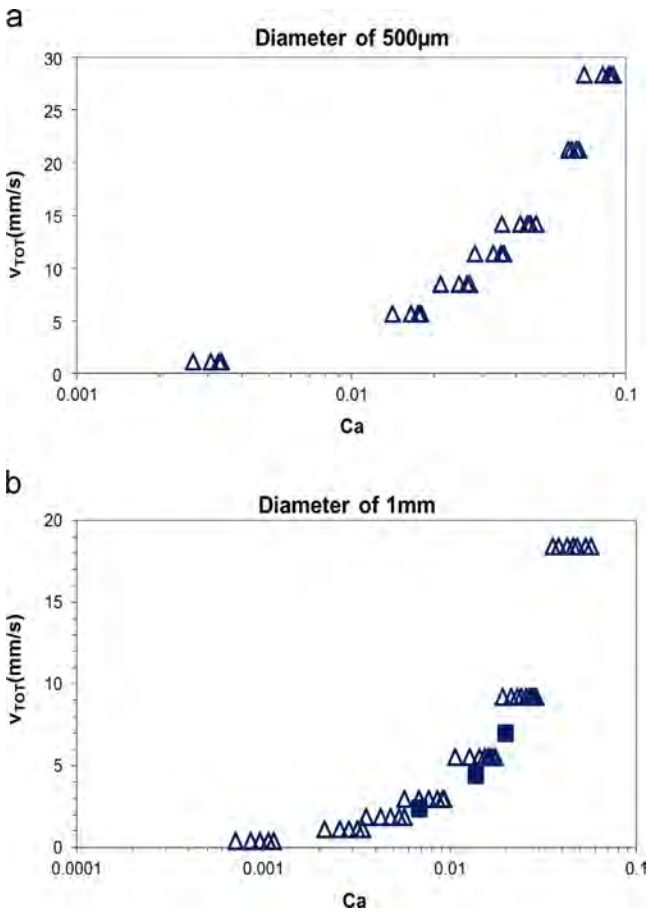

Fig. 2. Plot of the total flow velocity v_{TOT} versus Ca for diameters of (a) 500 μm and (b) 1 mm from 3D-experiments (open symbols) and 2D-simulations (square filled symbols).

magnitude. Then for a given Q_{TOT}, i.e. v_{TOT}, the protocol consists in varying the flow rate ratio (Q_D/Q_C) and so the flow velocity ratio (v_D/v_C) from 0.1 to 0.8. Therefore, v_C is varied in almost two orders of magnitude. As different regimes of droplet generation are observed in the literature according to the capillary number Ca, experimental and simulation conditions are represented in Fig. 2 by plotting the explored values of v_{TOT} versus Ca. Here, we limit the simulations to three total flow velocities and flow velocity ratios for a channel of 1 mm diameter (Fig. 2b), due to numerical calculation time. Fig. 2 shows that Ca is explored over a wide range which surrounds the critical value of 0.01–0.015 described in the literature to represent the importance of shear stresses on interfacial forces (Thorsen et al., 2001; Garstecki et al., 2006; Xu et al., 2008; Christopher et al., 2008; Liu and Zhang, 2009; Van Steijn et al., 2010; Tice et al., 2003; Zhao and Middelberg, 2011). However Ca is based on the continuous phase only. Hence Ca is not enough to characterize the flow regime as a Ca value can be obtained for different v_D and so different v_{TOT}. Therefore we have also explored different values of v_{TOT} for the same Ca by varying v_D while keeping v_C constant.

3.2. Observation of droplet formation regimes with 3D-experiments and 2D-simulations

Experimental results obtained with 3D microfluidics using channels of 500 μm diameter are compared with 2D simulations using channels of 1 mm diameter, in Fig. 3. In experimental results (Fig. 3a, c and e), ethanol plugs were generated and transported by the flow of oil in a transparent ETFE (Ethylene tetrafluoroethylene, a fluorine-based plastic from IDEX Health and Science catalog) T-junction. The observations were made under an optical microscope (Zeiss Axio Observer D1) equipped with a camera sCMOS (Neo, ANDOR Technology).

In experiments of Fig. 3a, c and e, different regimes of droplet formation are observed for a given v_D/v_C, depending on Ca value:

- Up to Ca=0.02, the droplet emerges in a hemispherical shape and the channel is filled by the dispersed phase as the droplet approaches the opposite wall. Then the droplet feeding proceeds making it grow in length before it forms a neck due to the flow of the continuous phase, which finally pulls it out. Hence the length of droplets is longer than W. This is the squeezing regime (Garstecki et al., 2006).
- When Ca is greater than 0.02, the flow of the continuous phase appears to compress the dispersed phase against the upper channel wall. In fact, due to the pressure exerted by the continuous phase, the dispersed phase forms a neck just after its outlet. For a given flow velocity, this neck becomes longer and thinner with increasing Ca, reducing droplet feeding before detachment. Hence droplets are shorter than W. This is called the dripping regime (Thorsen et al., 2001).
- At high values of Ca (near 0.2), a jet of the dispersed phase is observed at the junction (first pictures, Fig. 3 Ca=0.2 and 0.24,) with droplets forming far away from the junction. The reason why the dispersed phase jet breaks is that the surface tension γ_{CD} is lower for droplets than for a cylinder, while having the same volume. These Rayleigh-Plateau instabilities make droplets form farther from the dispersed phase outlet, and with a greater diameter, as the value of v_{TOT} increases. Therefore jet length increases with v_{TOT}. This is the jetting regime (De Menech et al., 2008). From our experiments, this jetting regime is obviously due to high values of both v_C and v_D.

Interestingly the simulations in Fig. 3b and d show that the behavior of phase flows qualitatively resembles that observed in experiments in similar conditions, even though the geometry is not perfect at the experimental junction. Moreover, simulations add the following information to experimental observations:

- In the dripping and the squeezing regimes, the droplet first emerges from the dispersed phase channel, and then grows until it detaches and moves under the pressure of the continuous phase.
- The transition Ca between dripping and jetting regimes decreases from 0.2 to 0.1 when (v_D/v_C) increases.
- The jetting regime appears to be correlated to total flow rate value v_{TOT} ($=v_D+v_C$), the transition occurring at v_{TOT} close to 50 mm s^{-1}. This value is observed experimentally for all ratios of flow velocities. Hence the continuous phase confines the dispersed phase near the upper wall, reducing jet diameter.

In conclusion, how Ca affects squeezing-to-dripping transition and how v_{TOT} affects dripping-to-jetting transition are clearly shown in Fig. 3. To our knowledge, how v_{TOT} affects the jetting regime is observed here for the first time. However, we do not aim for droplets smaller than W diameter because of the risk of coalescence due to their mobility in the tubing. Therefore, in the quantitative comparisons of our results below, we will focus on squeezing and dripping regimes.

3.3. Quantitative comparison of 3D-experiments and 2D-simulations

For quantitative comparison between 2D simulations and 3D experimental results, two parameters are explored in this work: droplet size and frequency (Fig. 4).

3.3.1. Droplet size

The experimental droplet length L is evaluated on pictures using the software ImageJ and L/W is calculated in order to compare results obtained with both channel diameters W. Fig. 4a represents L/W versus (v_D/v_C) for given values of v_{TOT}. For each value of (v_D/v_C) and v_{TOT}, L is measured on roughly one hundred droplets. Simulations are carried out for 1 mm channel diameters and values of L/W are consistent with those measured in 3D experiments for given (v_D/v_C) and v_{TOT}.

In Fig. 4a, values of L/W increase linearly with (v_D/v_C) as reported in the literature for L versus flow rate ratio Q_D/Q_C (Garstecki et al., 2006; Christopher et al., 2008; Liu and Zhang, 2009; Van Steijn et al., 2010; Tice et al., 2003). Our study is consistent with the literature because we define velocities by the ratio between flow rates and channel diameter, leading to (v_D/v_C) values equal to (Q_D/Q_C). However the linear fitting curves of L/W obviously depend on v_{TOT}. This is confirmed by 2D simulations at (v_D/v_C) of 0.2, which lead to distinct values of L/W due to different values of v_{TOT}.

Note that droplets of similar size to the channel diameter or smaller ($L/W \leq 1$) are generated with high values of v_{TOT} and low values of (v_D/v_C). Moreover, for v_{TOT} values higher than 7 mm/s, the dependence of droplet size on v_{TOT} is less marked. In fact, it corresponds to the dripping regime observed in Fig. 3 at Ca > 0.015, where the presence of a neck reduces droplet feeding. Hence the dependence on v_D/v_C is also reduced.

3.3.2. Droplet frequency

In the literature, droplet frequency, defined as the number of droplets per second, is given by the ratio between the flow rate of the dispersed phase and the volume of droplets in a steady regime, in order to conserve the mass of the dispersed phase. As our aim is to represent a flow by its velocity, we define the droplet frequency f_D as the production rate of a dispersed phase of L length due to injection at a velocity v_D. Hence f_D is given by:

$$f_D = \frac{v_D}{L} \tag{8}$$

Fig. 4b represents f_D measurements, varying (v_D/v_C) and v_{TOT} in experiments with both W values and in simulations with 1 mm

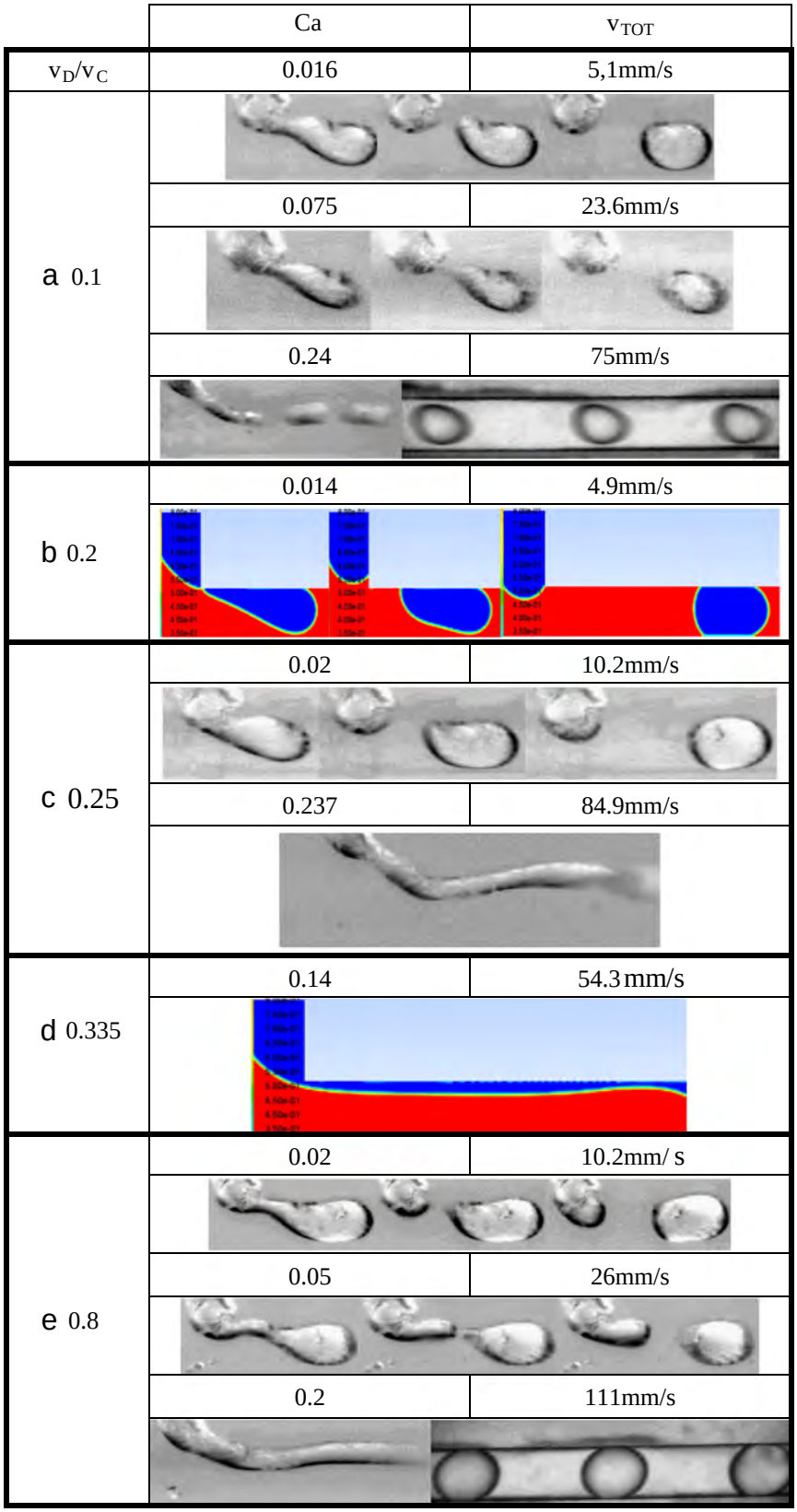

Fig. 3. (a), (c) and (e): droplet formation in 3D-experiments using channels of 500 μm diameter; (b) and (d): droplet formation in 2D-simulations using channels of 1 mm diameter.

channel diameter. As for L/W, f_D values obtained in 2D simulations are consistent with f_D measured in 3D experiments for given (v_D/v_C) and v_{TOT}.

Furthermore, f_D values increase as a power-law of (v_D/v_C) as reported in the literature for f_D versus flow rate ratio Q_D/Q_C[18]. However the fitting curves of f_D obviously depend on v_{TOT}. This is

confirmed by simulations at (v_D/v_C) of 0.2, which lead to distinct values of L/W due to different values of v_{TOT}.

In conclusion, 3D experimental and 2D simulation results taken together confirm that it is relevant to interpret experimental results through flow velocities, even though the geometry is cylindrical at the experimental T-junction. Moreover, the average velocity of flows being defined proportional to flow rates in this paper, it is easy to compare with flow rates in the literature. We not only observe that L/W and f_D are influenced by (v_D/v_C) as described in the literature but our experimental and simulation results also show clearly that v_{TOT} plays a significant role in the generation of droplets. This contribution of v_{TOT} through the absolute values of v_D and v_C is described thoroughly in Section 4 of this paper.

4. Discussion

4.1. Is v_D/v_C alone sufficient to describe L/W?

According to Sections 3.2 and 3.3, L/W is influenced by v_D/v_C, as found in the literature. However, it is obvious that the parameters v_{TOT} and Ca also play a role in droplet formation. Therefore, we start the investigation by exploring the influence of v_{TOT} and Ca, in addition to v_D/v_C on L/W.

4.1.1. Influence of v_{TOT} on droplet size in addition to (v_D/v_C)

Fig. 4a shows that experimental results of L/W, obtained with 500 μm and 1 mm channel diameters (W), indicate a linear increase of L/W with (v_D/v_C). These linear fitting curves involve two parameters, a slope $\boldsymbol{\alpha}$ and an initial value $\boldsymbol{\beta}$ (for $v_D/v_C=0$) that corresponds to the minimum droplet length:

$$\frac{L}{W}=\boldsymbol{\alpha}\frac{v_D}{v_C}+\boldsymbol{\beta} \tag{9}$$

In the literature, the linear relationship between L/W and (Q_D/Q_C) was described in rectangular channels only for the squeezing regime for Ca < 0.01 (Garstecki et al., 2006; Christopher et al., 2008; Liu and Zhang, 2009; Van Steijn et al., 2010). In contrast, in our work the linear relationship is valid for all explored Ca values, from 0.001 to 0.1, and thus for both squeezing and dripping regimes (Fig. 3). Moreover, the variation of L/W is explained in the literature essentially by the influence of (Q_D/Q_C), with fixed values of $\boldsymbol{\alpha}$ and $\boldsymbol{\beta}$ (in the order of 1 for Garstecki et al. (2006)). In our case, both $\boldsymbol{\alpha}$ and $\boldsymbol{\beta}$ decrease linearly with v_{TOT} (Fig. 5a), with two slopes depending on the range of v_{TOT}. The slope change occurs at a similar v_{TOT} value for both $\boldsymbol{\alpha}$ and $\boldsymbol{\beta}$, i.e. 9–10 mm/s and 4–5 mm/s for 500 μm and 1 mm diameters respectively (Fig. 5a). The value of $\boldsymbol{\beta}$ at the intercept of the two slopes is close to 1, meaning that the droplet length is close to the channel diameter. In fact two droplet regimes are generated with two slopes for α and β variations, depending on v_{TOT} value:

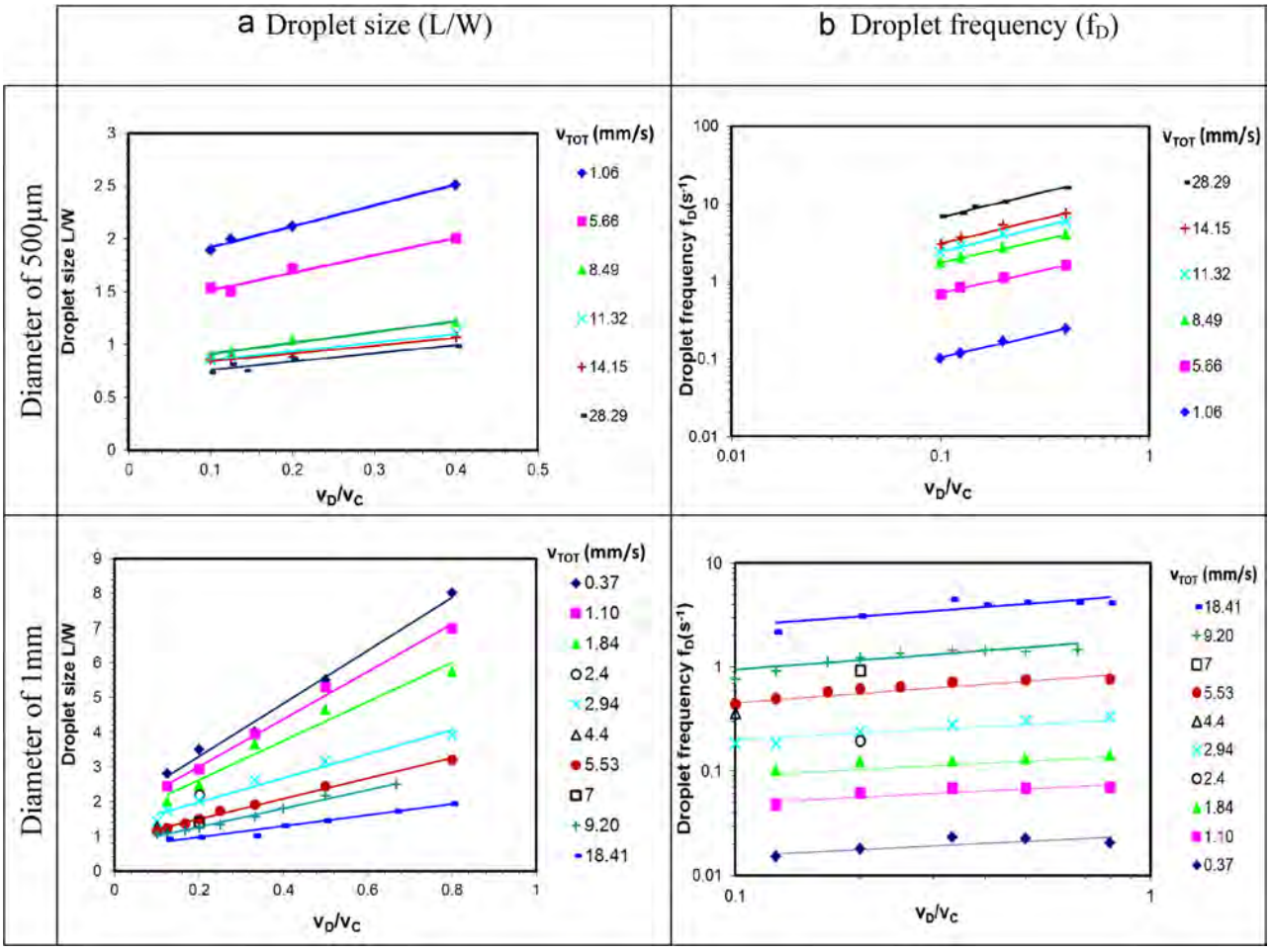

Fig. 4. Plots of (a) droplet size (L/W) and (b) droplet frequency (f_D) versus (v_D/v_C) for given v_{TOT} from: 3D experiments for channel diameters of 500 μm and 1 mm and 2D simulations for a channel diameter of 1 mm (open symbols).

- For low v_{TOT}, $\boldsymbol{\beta}$ is higher than 1, meaning that whatever the value of (v_D/v_C), the droplet is detached only after its diameter has reached the channel diameter and the droplet has further expanded length-wise. Hence even for low values of v_D, v_C is low enough to let the dispersed phase fill the channel cross-section. The evaluation of Ca related to low v_{TOT} (Fig. 2) leads to Ca < 0.01–0.015, corresponding to the squeezing regime in the literature. Our experimental results show that in this regime, both $\boldsymbol{\alpha}$ and $\boldsymbol{\beta}$ vary considerably with v_{TOT} (Figs. 4a and 5a).
- For high v_{TOT}, $\boldsymbol{\beta}$ is lower than 1, meaning that at low values of (v_D/v_C), the droplet can detach before its diameter has reached the channel diameter. Hence even for high values of v_D the dispersed phase does not fill the channel cross-section because v_C is also very high. Here, Ca is higher than 0.01–0.015, corresponding to the dripping regime. Our experimental results show that in this regime, $\boldsymbol{\alpha}$ and $\boldsymbol{\beta}$ are less influenced by v_{TOT} and v_D/v_C (Figs. 4a and 5a).

The linear relationship with (v_D/v_C) and the two regimes observed depending on the Ca value are in accordance with the literature. However L/W values are obviously influenced by v_{TOT}, i.e. absolute values of v_C and v_D. Moreover two different values of (v_D/v_C) can give the same L/W if v_{TOT} varies in the right way (Fig. 4a). We thus seek to merge (v_D/v_C) and v_{TOT} influences by plotting L/W versus $[(v_D/v_C)/v_{TOT}]$ (Fig. 5b).

The curves are fitted to the scaling law:

$$\frac{L}{W} = \left(K_1 \times \frac{v_D/v_C}{v_{TOT}}\right)^m \tag{10}$$

The value of m is proportional to the channel diameter (1/4 for 500 μm and 1/2 for 1 mm) leading to an increasing influence of $[(v_D/v_C)/v_{TOT}]$ on L/W with increasing channel diameter. It is

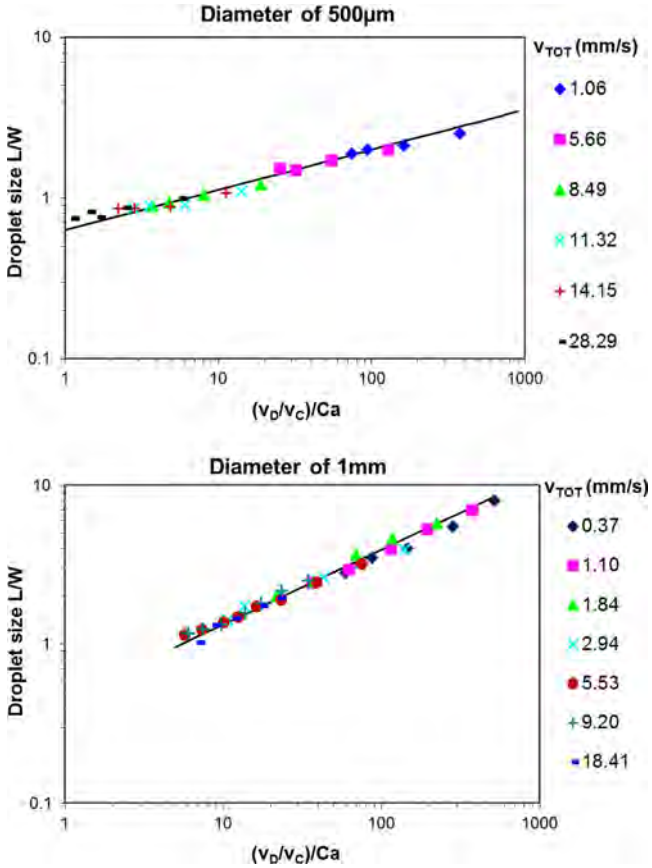

Fig. 6. Plot of L/W versus $[(v_D/v_C)/Ca]$ for 500 μm and 1 mm channel diameters.

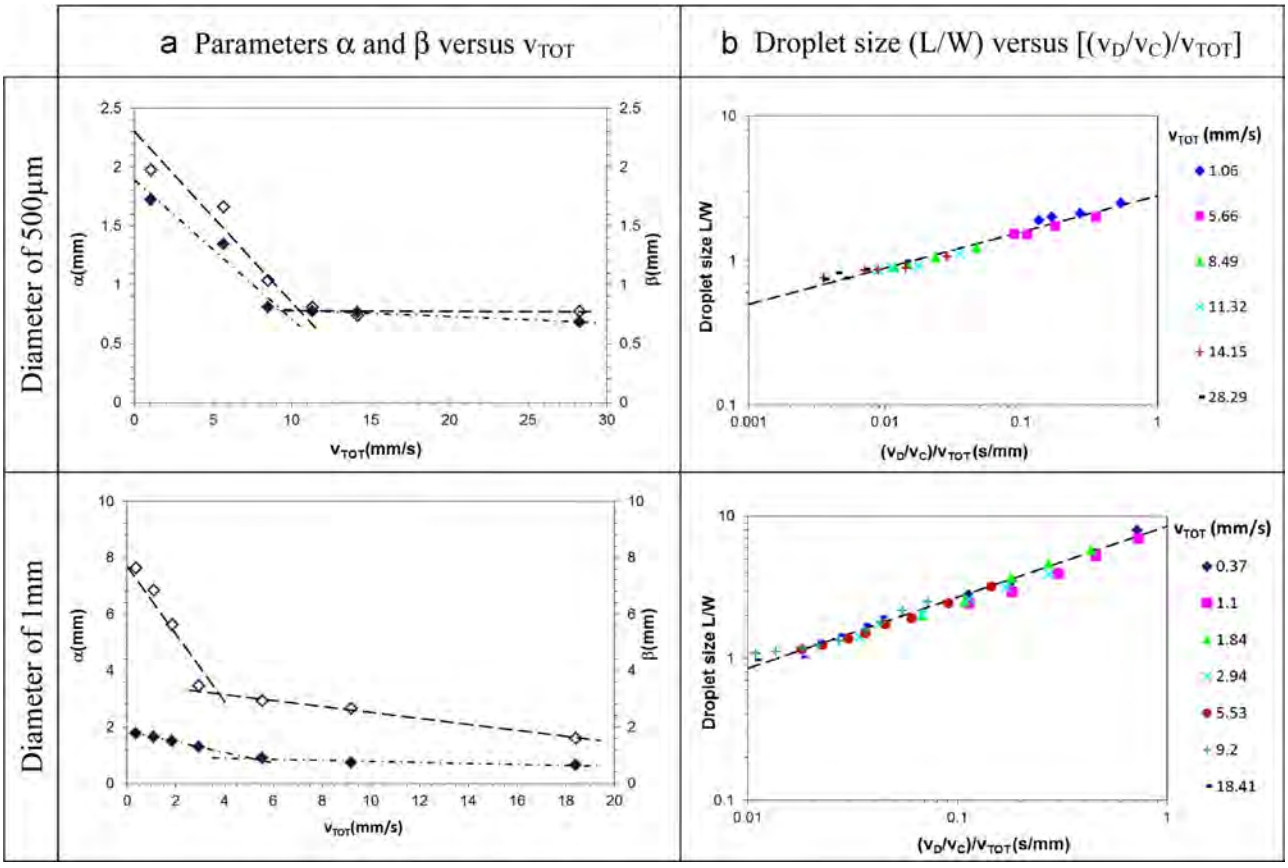

Fig. 5. Plot of (a) parameters $\boldsymbol{\alpha}$ (open symbols) and $\boldsymbol{\beta}$ (filled symbols) versus v_{TOT} and (b) droplet size (L/W) versus $[(v_D/v_C)/v_{TOT}]$, for channel diameters of 500 μm and 1 mm.

noteworthy that the pre-factor K_1 is similar (68 mm/s) for both channel diameters. Hence, in addition to the flow rate ratio, the total flow rate permits droplet size to be adjusted from shorter to longer than the channel diameter. Here therefore, mono-dispersed droplets can be produced at a variety of (v_D/v_C) values, by keeping the ratio $[(v_D/v_C)/v_{TOT}]$ constant. On the other hand, droplets of different sizes can be produced by keeping (v_D/v_C) constant while varying $[(v_D/v_C)/v_{TOT}]$. For our application, the value of K_1 can be considered as a characteristic velocity which defines the operating range permitting droplets to mix without coalescence, as explained in Section 1.

However, this relationship does not take into account the physico-chemical properties of the two phases, i.e. the viscosity μ_C and the surface tension γ_{CD}. Moreover Garstecki et al. (2006) showed that for the squeezing regime (low Ca values), the scaling relation giving L/W is independent of phase properties. Nevertheless, as two regimes of droplet generation are observed depending on Ca values, phase properties must play a role in droplet size.

4.1.2. *Influence of Ca on droplet size in addition to (v_D/v_C)*

L/W is shown above to increase with (v_D/v_C) (Fig. 4a). Hence we assume that the influence of Ca on L/W is combined with the influence of (v_D/v_C) by plotting L/W versus $[(v_D/v_C)/Ca]$, for given v_{TOT} (Fig. 6). Fig. 6 shows how all the results for each channel diameter can be combined so that the fitting curves correspond to a scaling law:

$$\frac{L}{W} = \left(K_2 \times \frac{v_D/v_C}{Ca}\right)^n \tag{11}$$

The value of n is proportional to the diameter (1/4 for 500 μm and 1/2 for 1 mm) leading to an increasing influence of $[(v_D/v_C)/Ca]$ on L/W as the diameter increases. It is noteworthy that the dimensionless pre-factor K_2 is similar (~19) for both channel diameters. Moreover, this empirical law is consistent with the literature for high values of Ca (0.05–1) (Xu et al., 2008; Christopher et al., 2008; Zhao and Middelberg, 2011). It is in accordance with the increase of L/W with the surface tension γ_{CD} observed by Wehking et al. (2013) and the decrease of L/W with the viscosity μ_C observed by Gupta and Kumar (2010). However, it must be noted that our relation is valid over a wider range of Ca, from 0.005 to 1.

Physico-chemical parameters γ_{CD} and μ_C are fixed here, and so can be moved to K_2. Hence it is interesting to note that relations (Eqs. (10) and (11)) depend on (v_D/v_C) with the same exponent values (m and n) depending on channel diameter. Moreover the parameters K_1 and K_2 do not depend on channel diameter. Thus these empirical laws can be determined for a given diameter if the absolute flow velocity and phase physico-chemical properties are known. Moreover as v_C value is fixed by Ca and v_D value by (v_{TOT}), droplet size may be related to v_{TOT} and Ca.

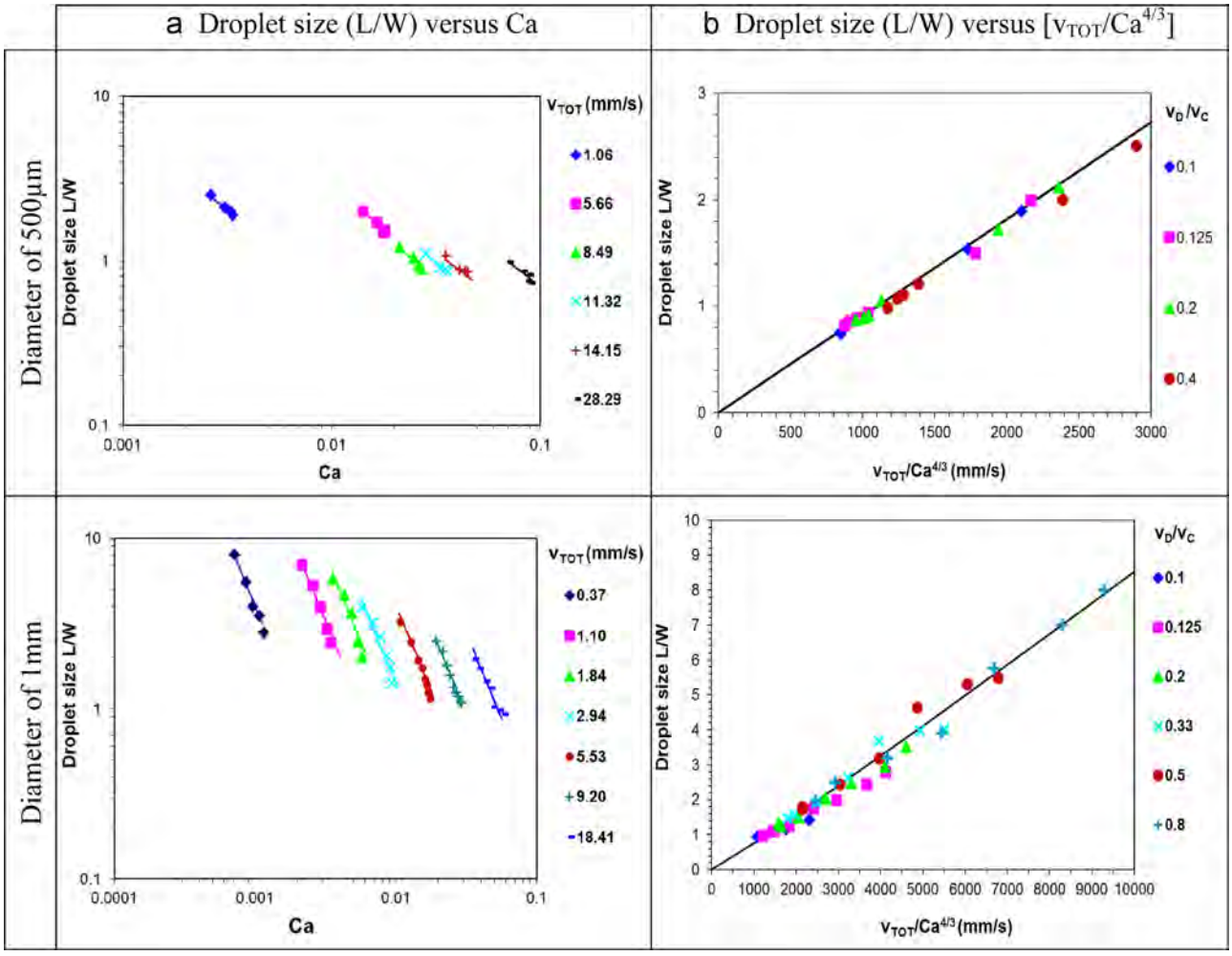

Fig. 7. Plot of droplet size (L/W) versus (a) the capillary number Ca for given v_{TOT} and (b) $[v_{TOT}/Ca^{4/3}]$ for given v_D/v_C, from experiments with of 500 μm and 1 mm channel diameters.

4.2. Influence of Ca and v_{TOT} without using (v_D/v_C)

As we have demonstrated that v_{TOT} and Ca, in addition to v_D/v_C, influence L/W, the remaining question is whether we can directly correlate L/W to v_{TOT} and Ca without using (v_D/v_C), and how this can be applied to droplet frequency?

4.2.1. Influence of Ca and v_{TOT} on droplet size

L/W was observed above to decrease with v_{TOT} (Fig. 4a). In order to explore the influence of Ca, we plot L/W versus Ca, for given v_{TOT} (Fig. 7a). In Fig. 7a for given v_{TOT}, L/W decreases with Ca and fitting curves depend on Ca and v_{TOT}:

$$\frac{L}{W} = \frac{v_{TOT}}{K_3 \times Ca^{4/3}} \tag{12}$$

Plotting L/W versus $[v_{TOT}/Ca^{4/3}]$ combines all the results obtained for different flow rate ratios v_D/v_C (Fig. 7b).

It is noteworthy that the pre-factor K_3 is similar (10^{-3} mm/s) for both channel diameters and it can be considered as a characteristic velocity which defines the operating range permitting droplets to mix without coalescence for our application. Therefore, this empirical law allows the prediction of L/W value for each given v_{TOT} and Ca. In the literature, droplet length is related either to flow rate ratio (Garstecki et al., 2006) or to continuous phase flow rate (Liu and Zhang, 2009). Here, the total velocity v_{TOT} contains the continuous phase velocity v_C and the dispersed phase velocity v_D, and the capillary number Ca contains v_C. Hence it is more important to know the absolute values of both velocities than the ratio (v_D/v_C). Moreover, because Ca depends on the viscosity μ_C and the surface tension γ_{CD}, their influence on L/W needs to be tested in future to check the validity of our law.

4.2.2. Application to droplet frequency

Fig. 4b shows that experimental results of droplet frequency f_D, obtained with 500 μm and 1 mm channel diameters, indicate that L/W increases with (v_D/v_C). However for a given (v_D/v_C), droplet frequency f_D also increases with v_{TOT}. Moreover our detailed investigation of L/W suggests that the parameter Ca plays a role in the frequency of droplet generation. Therefore, we plot f_D versus $[v_{TOT}/Ca^{4/3}]$ for given v_D/v_C (Fig. 8) (as above for L/W).

The fitting curves in Fig. 8 correspond to a scaling law:

$$f_D \propto \left(\frac{v_{TOT}}{Ca^{4/3}}\right)^p \tag{13}$$

For both channel diameters, it is noteworthy that the value of p is identical (~ -4). Moreover the factor f_D increases with (v_D/v_C) and it decreases with channel diameter.

The droplet frequency in T-junction microfluidics has rarely been studied, even though the definition of f_D (v_D/L) makes it easy to calculate using the experimental results of the literature. However, Christopher et al. (2008) and Gupta and Kumar (2010) also showed that f_D scales with $Ca^{4/3}$. Nevertheless, Gupta and Kumar (2010) varied the diameter ratio (W_D/W_C) between the channels of the dispersed phase and the continuous phase, and observed that f_D is influenced by this ratio, but not by the absolute value of channel diameters. Here, the ratio (W_D/W_C) is equal to 1 and we note that for given values of Ca, v_D and v_{TOT}, f_D is inversely proportional to channel diameters W (Fig. 8).

For our application, the operating range permitting droplets to mix without coalescence, as explained in Section 1, corresponds experimentally to L/W near a value of 1 and low values of f_D:

- For $L/W \approx 1$, $[v_{TOT}/Ca^{4/3}]$ must be 1000 mm/s for both diameters (Fig. 7b).

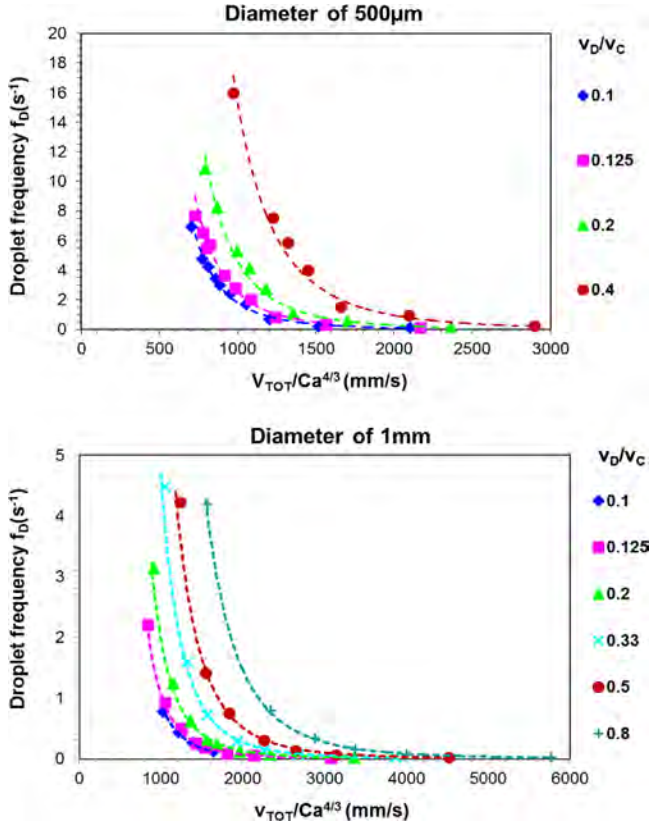

Fig. 8. Plot of droplet frequency f_D versus $[v_{TOT}/Ca^{4/3}]$ for given v_D/v_C, from experiments with 500 μm and 1 mm channel diameters.

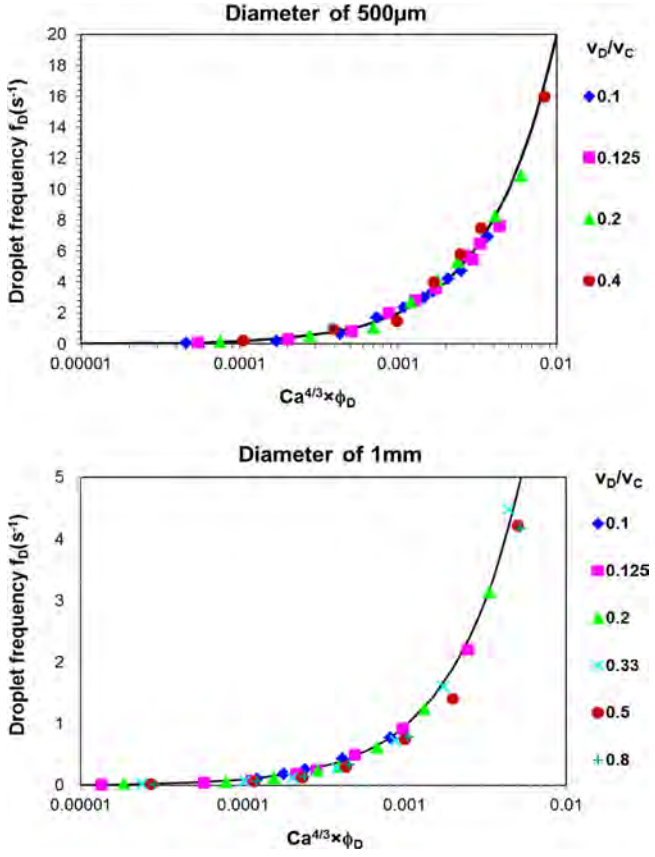

Fig. 9. Plot of f_D versus $(Ca^{4/3} \times \phi_D)$ for given (v_D/v_C), from experiments with 500 μm and 1 mm channel diameters.

- For $[v_{TOT}/Ca^{4/3}]$ of 1000 mm/s, f_D increases with (v_D/v_C) and this increase is enhanced, thereby increasing the risk of coalescence, when the diameter is reduced (Fig. 8).

Thus for a given v_C(mm/s), v_D(mm/s) is first calculated for $[v_{TOT}/Ca^{4/3}]$ equal to 1000. This yields a ratio (v_D/v_C) permitting droplet frequency to be evaluated graphically (Fig. 8).

For a given v_D, an easy way to evaluate v_C is by introducing the ratio (v_D/v_{TOT}) which corresponds to "the fraction of dispersed phase" ϕ_D as defined by Tice et al. (2003) in mixing studies. This ratio appears in the relation of f_D, with Ca and v_{TOT} resulting from Eq. (12):

$$f_D = \frac{K_4 \times Ca^{\frac{4}{3}}}{W} \times \frac{v_D}{v_{TOT}} \quad (14)$$

Then by plotting f_D versus $(Ca^{4/3} \times \phi_D)$ all the results obtained for different flow rate ratios (v_D/v_C) can be combined with pre-factor K_4 value of 1000 mm/s for both channel diameters. In our application, as $[v_{TOT}/Ca^{4/3}]$ is equal to 1000 mm/s, K_4 can be considered as a characteristic velocity which defines the operating range permitting droplets to mix without coalescence. v_D can be chosen (without knowing v_C) so as to obtain the desired f_D using Eq. (14), and hence different ratios (v_D/v_C). Finally Fig. 9 shows how the operational range of (v_D/v_C) can be broadened.

In conclusion, for practical applications L/W and f_D can be predicted with given pairs of absolute values (v_{TOT} and v_D or v_C) or (v_D and v_C), using Eqs. (12) and (14), respectively. Moreover, we can define the operating range for these pairs of parameters for a given v_D in order to generate homogeneous droplets with droplet size similar to the channel diameter and low frequency.

5. Conclusion

This paper presents a hydrodynamic study of our microfluidic system used for crystallization studies (Ildefonso et al., 2012), which is based on a T-junction with two channels of circular cross-section with the same diameter. Firstly, 3D experiment and 2D simulation results obtained in this work confirm that our cylindrical microfluidic channels can be compared to the planar geometries with rectangular cross-section described in the literature. Therefore the displacement of phases in our 3D cylindrical channels can be represented by the average flow velocity instead of the flow rate. Secondly, this study investigates the influence of the total flow velocity v_{TOT} and the capillary number Ca, in addition to the flow velocity ratio (v_D/v_C), on droplet generation. We thus demonstrate, for the first time, that the flow velocity ratio (v_D/v_C) is not sufficient to predict droplet size and frequency; and that the total flow velocity v_{TOT} or the absolute flow velocity values v_D and v_C are required. Hence, we establish empirical laws predicting droplet size and frequency with v_D, v_C and Ca. These correlations allow us to define the operating range that will generate homogeneous droplets. Moreover, our results are obtained for channel diameters of 500 μm and 1 mm, which are one order of magnitude larger than that usually tested in the literature (between 50 and 300 μm), while remaining smaller than the capillary length (2.4 mm).

Nomenclature

Ca	Capillary number $(\mu_C \times v_C/\gamma_{CD})$ (dimensionless)
d	Distance between 2 droplets (m)
f	Frequency (s^{-1})
g	Gravity acceleration (m/s^2)
K_1	Proportionality factor (m/s)
K_2	Proportionality factor (dimensionless)
K_3	Proportionality factor (m/s)
K_4	Proportionality factor (m/s)
L	Droplet length (m)
l_c	Capillary length $([\gamma_{CD}/(\Delta\rho \times g)]^{1/2})$ (m)
m	Power factor (dimensionless)
n	Power factor (dimensionless)
$\vec{n}$	Outward normal vector of the interface (dimensionless)
p	Power factor (dimensionless)
Q	Flow rate (m^3/s)
Re	Reynolds number $(\rho_C \times v_C \times (W/2)/\mu_C)$ (dimensionless)
v	Absolute flow velocity (m/s)
W	Channel diameter (m)

Greek symbols

α	Slope (dimensionless)
β	Initial value (dimensionless)
$\Delta\rho$	Difference in density (kg/m^3)
ϕ	Volume fraction (dimensionless)
γ	Surface tension (N/m)
κ	Curvature of the interface (m)
μ	Dynamic viscosity(Pa s)
ρ	Density (kg/m^3)

Subscripts

C	Continuous phase
D	Dispersed phase
TOT	Total (continuous and dispersed phases)

Acknowledgments

We thank M. Sweetko for English revision and the laboratory IRPHE for access to computational phase dynamics package Fluent.

Appendix A. Supporting information

Supplementary data associated with this article can be found in the online version at http://dx.doi.org/10.1016/j.ces.2015.07.046.

References

Anna, S.L., Bontoux, N., Stone, H.A., 2003. Formation of dispersions using flow focusing in microchannels. Appl. Phys. Lett. 82 (3), 364–366.
Brouzes, E., Medkova, M., Savenelli, N., Marran, D., Twardowski, M., Hutchison, J.B., Rothberg, J.M., Link, D.R., Perrimon, N., Samuels, M.L., 2009. Droplet microfluidic technology for single-cell high-throughput screening. Proc. Natl. Acad. Sci. 106 (34), 14195–14200.
Bukiet, F., Couderc, G., Camps, J., Tassery, H., Cuisinier, F., About, I., Charrier, A., Candoni, N., 2012. Wetting properties and critical micellar concentration of benzalkonium chloride mixed in sodium hypochlorite. J. Endod. 38 (11), 1525–1529.
Burns, M.A., Johnson, B.N., Brahmasandra, S.N., Handique, K., Webster, J.R., Krishnan, M., Sammarco, T.S., Man, P.M., Jones, D., Heldsinger, D., Mastrangelo, C.H., Burke, D.T., 1998. An integrated nanoliter DNA analysis device. Science 282 (5388), 484–487.
Candoni, N., Hammadi, Z., Grossier, R., Ildefonso, M., Revalor, E., Ferté, N., Okutsu, T., Morin, R., Veesler, S., 2012. Nanotechnologies dedicated to nucleation control. Int. J. Nanotechnol. 9 (3–7), 439–459.
Chen, N., Wu, J., Jiang, H., Dong, L., 2011. CFD simulation of droplet formation in a wide-type microfluidic T-junction. J. Dispers. Sci. Technol. 33 (11), 1635–1641.
Christopher, G.F., Noharuddin, N.N., Taylor, J.A., Anna, S.L., 2008. Experimental observations of the squeezing-to-dripping transition in T-shaped microfluidic junctions. Phys. Rev. E 78 (3), 036317.
De Menech, M., Garstecki, P., Jousse, F., Stone, H.A., 2008. Transition from squeezing to dripping in a microfluidic T-shaped junction. J. Fluid Mech. 595, 141–161.

Gañán-Calvo, A.M., Gordillo, J.M., 2001. Perfectly monodisperse microbubbling by capillary flow focusing. Phys. Rev. Lett. 87 (27), 274501.
Garstecki, P., Stone, H.A., Whitesides, G.M., 2005. Mechanism for flow-rate controlled breakup in confined geometries: a route to monodisperse emulsions. Phys. Rev. Lett. 94 (16), 164501.
Garstecki, P., Fuerstman, M.J., Stone, H.A., Whitesides, G.M., 2006. Formation of droplets and bubbles in a microfluidic T-junction-scaling and mechanism of break-up. Lab Chip 6 (3), 437–446.
Glawdel, T., Elbuken, C., Ren, C.L., 2012a. Droplet formation in microfluidic T-junction generators operating in the transitional regime. II. Modeling. Phys. Rev. E 85 (1), 016323.
Glawdel, T., Elbuken, C., Ren, C.L., 2012b. Droplet formation in microfluidic T-junction generators operating in the transitional regime. I. Experimental observations. Phys. Rev. E 85 (1), 016322.
Gupta, A., Kumar, R., 2010. Flow regime transition at high capillary numbers in a microfluidic T-junction: viscosity contrast and geometry effect. Phys. Fluids 22, 12.
Ildefonso, M., Candoni, N., Veesler, S., Cheap, A, 2012. Easy microfluidic crystallization device ensuring universal solvent compatibility. Org. Process Res. Dev. 16, 556–560.
Li, L., Ismagilov, R.F., 2010. Protein crystallization using microfluidic technologies based on valves, droplets, and slipchip. Annu. Rev. Biophys. 39 (1), 139–158.
Li, L., Mustafi, D., Fu, Q., Tereshko, V., Chen, D.L., Tice, J.D., Ismagilov, R.F., 2006. Nanoliter microfluidic hybrid method for simultaneous screening and optimization validated with crystallization of membrane proteins. Proc. Natl. Acad. Sci. 103 (51), 19243–19248.
Liu, H., Zhang, Y., 2009. Droplet formation in a T-shaped microfluidic junction. J. Appl. Phys. 106, 3.
Nisisako, T., Torii, T., Higuchi, T., 2002. Droplet formation in a microchannel network. Lab Chip 2 (1), 24–26.
Selimovic, S., Jia, Y., Fraden, S., 2009. Measuring the nucleation rate of lysozyme using microfluidics. Cryst. Growth Des. 9 (4), 1806–1810.
Thorsen, T., Roberts, R.W., Arnold, F.H., Quake, S.R., 2001. Dynamic pattern formation in a vesicle-generating microfluidic device. Phys. Rev. Lett. 86 (18), 4163–4166.
Tice, J.D., Song, H., Lyon, A.D., Ismagilov, R.F., 2003. Formation of droplets and mixing in multiphase microfluidics at low values of the reynolds and the capillary numbers. Langmuir 19 (22), 9127–9133.
Umbanhowar, P.B., Prasad, V., Weitz, D.A., 1999. Monodisperse emulsion generation via drop break off in a coflowing stream. Langmuir 16 (2), 347–351.
Van Steijn, V., Kleijn, C.R., Kreutzer, M.T., 2010. Predictive model for the size of bubbles and droplets created in microfluidic T-junctions. Lab Chip 10 (19), 2513–2518.
Wehking, J., Gabany, M., Chew, L., Kumar, R., 2013. Effects of viscosity, interfacial tension, and flow geometry on droplet formation in a microfluidic T-junction. Microfluid Nanofluid, 1–13.
Xu, J.H., Li, S.W., Tan, J., Luo, G.S., 2008. Correlations of droplet formation in T-junction microfluidic devices: from squeezing to dripping. Microfluid Nanofluid 5 (6), 711–717.
Zare, R.N., Kim, S., 2010. Microfluidic platforms for single-cell analysis. Annu. Rev. Biomed. Eng. 12 (1), 187–201.
Zhao, C.-X., Middelberg, A.P.J., 2011. Two-phase microfluidic flows. Chem. Eng. Sci. 66 (7), 1394–1411.